*Optica Applicata, Vol. LII, No. 3, 2022*
DOI: 10.37190/oa220301

# Analysis of nonlinear parity-time symmetric four-layer Bragg grating

PIOTR WITOŃSKI*, AGNIESZKA MOSSAKOWSKA-WYSZYŃSKA

Institute of Microelectronics and Optoelectronics, Warsaw University of Technology, Koszykowa 75, 00-662 Warsaw, Poland

*Corresponding author: P.Witonski@elka.pw.edu.pl

The one dimensional PT (parity time) symmetric four-layer Bragg grating with gain and loss saturation effects is analyzed taking into account the evolution of the field amplitudes. The investigated structure has modulated real and imaginary parts of refractive index. The functional configurations of the Bragg grating have been considered, showing the behavior of this structure acting as a discrete device and as a component of an integrated circuit. The obtained characteristics illustrate the influence of the saturation effect on the intensity of the output wave at a given intensity of the incident plane wave for different values of gain and loss saturation intensities of the PT structure. The performed analysis shows the bistability of the structure and a strong influence of the incident wave intensity on the properties of light propagation nonreciprocity.

Keywords: integrated optics, nonlinear optics, Bragg grating, parity time.

## 1. Introduction

A study of parity-time (PT)-symmetric structures began in 1998 [1]. It was shown that even non-Hermitian Hamiltonians can exhibit entirely real spectra as long as they fulfill the conditions of PT-symmetry. In photonics, PT-symmetric devices are created from artificial materials with balanced gain and loss regions. These one-dimensional nonreciprocal structures, being a type of Bragg grating, have, inter alia, the following features: unidirectional invisibility [2], coherent perfect absorption [3], nonreciprocity of light propagation and beam refraction [4].

Such PT gratings were first explored in [5]. They are composed as periodic structures of $N$ two-layers primitive cells. Every cell is formed of a gain (amplifying) and loss (absorbing) layer. Their complex indices of refraction, along the optical $z$-axis, satisfy the condition $n^*(-z) = n(z)$, where the asterisk denotes a complex conjugate. PT structures are made in various configurations of the gain and loss layers [6], as well as in systems with additional modulation of the real part of refractive indices [7]. These structures have various applications, *e.g.* as a Bragg grating [8], in lasers as an ampli-

fying medium [9], and also as an output mirror [10], where they provide better energy efficiency of the laser [11]. Nonlinear PT structures with modulated real and imaginary refractive index parts, where the saturation effect of the gain was taken into account, were first studied in [7]. The authors showed modeling (in the time domain) of an optical switch built from a symmetrical PT grating using TLM method, but without taking into account the evolution of the field amplitudes in the cell.

In this paper, the authors extend the analysis from [12] by introducing an additional modulation of the real part of the refractive index of PT structures. Next, they take into account the influence of the media surrounding such grating on its transmission properties. Typical parameters of InP devices, which are commonly used for the production of integrated photonic circuits [13] and optical telecommunications devices [14], were adopted for the numerical analysis. In optical PT structures, gain and loss are controlled by a selectively applied bias voltage [15]. This approach makes it possible to analyze the output wave intensity of the finite PT structures as a function of the incident wave intensity and different saturation levels of gain and loss (the infinite structure has already been analyzed in [12]).

The analysis of the nonlinear PT Bragg grating with modulated refractive index was performed for four configurations. In the first one, the PT structure is a discrete device surrounded by air. In the second configuration, the structure is an element of an integrated circuit made of InP. In the third and fourth configurations, the PT structure is a device used, for example, in integrated opto-electronics. The study is performed for a wavelength typical for telecommunications systems: $\lambda = 1.55$ μm. The nonlinear PT Bragg grating was analyzed using a modified transition matrix method [16]. The proposed model allowed to study the influence of different levels of gain and loss saturation on the output wave intensity of PT structures with modulated real and imaginary refractive index in four different configurations.

## 2. Theoretical analysis

The investigated PT structure with modulation of the real refractive index in gain and loss layers is shown in Fig. 1**a**. It is a periodic structure, composed of primitive cells constructed of four layers: two amplifying and two absorbing, with widths $a$ and $b$, $c$ and $d$, respectively. These widths are equal to each other, $a = b = c = d$, and their sum is the period of the PT structure $\Lambda = a + b + c + d$. The length of the analyzed system is equal to $L = N\Lambda$, where $N$ is the number of primitive cells.

The gain and loss layers are characterized by complex refractive indices with opposite sign imaginary parts. The refractive indices of the primitive cell for the four investigated layers are described as follows:

$$n_1 = n_{1\mathrm{R}} - jn_{1\mathrm{I}} = n_0 + \Delta n_{\mathrm{R}} - jn_{\mathrm{I}} \tag{1a}$$

$$n_2 = n_{2\mathrm{R}} - jn_{2\mathrm{I}} = n_0 - \Delta n_{\mathrm{R}} - jn_{\mathrm{I}} \tag{1b}$$

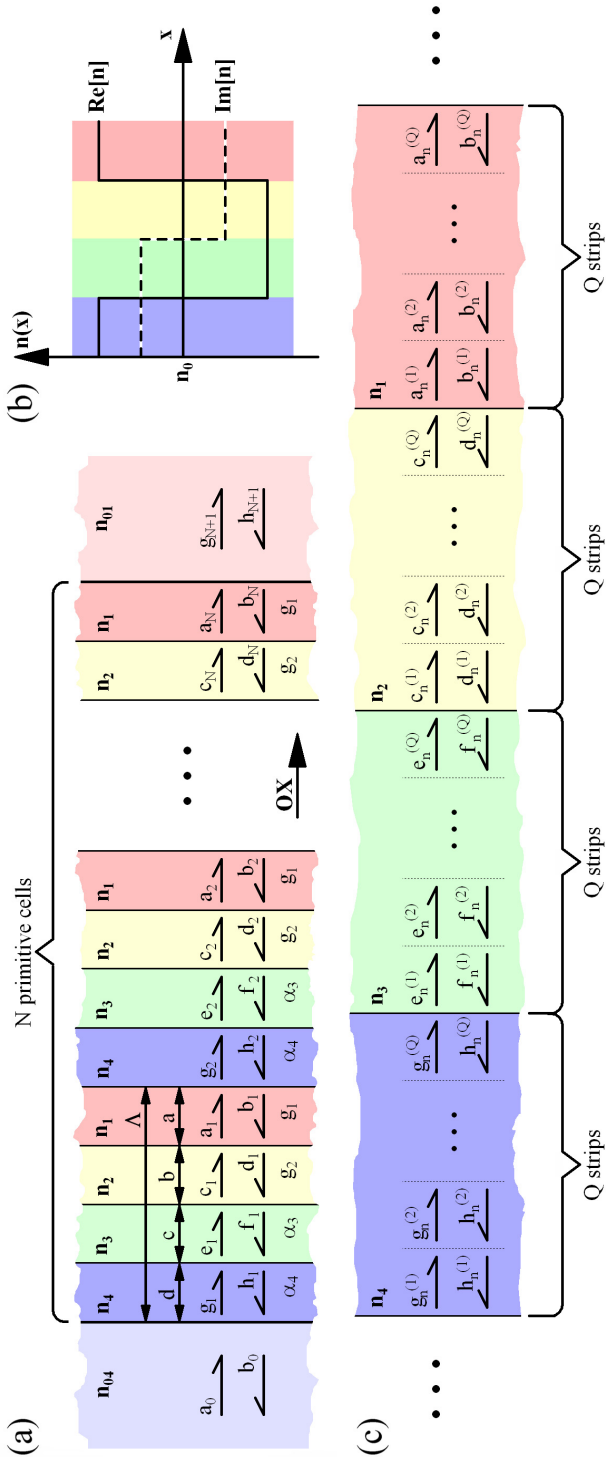


Fig. 1. (**a**) Investigated PT structure. (**b**) Distribution of the complex refractive index in a primitive cell. (**c**) Scheme of the *n*-th PT primitive cell divided into sublayers.

$$n_3 = n_{3R} + jn_{3I} = n_0 - \Delta n_R + jn_I \tag{1c}$$

$$n_4 = n_{4R} + jn_{4I} = n_0 + \Delta n_R + jn_I \tag{1d}$$

where $n_1$ and $n_2$ are the refractive indices of the gain layers, $n_3$ and $n_4$ are the refractive indices of the loss layers, their real parts are denoted as $n_{1R}$, $n_{2R}$, $n_{3R}$ and $n_{4R}$. $n_0$ is a constant component of the real part of all refractive indices and the parameter $\Delta n_R$ is its change. The imaginary parts of the refractive index are described as $n_{1I}$, $n_{2I}$, $n_{3I}$ and $n_{4I}$. The distribution of the real and imaginary part of the refractive index along the $x$-axis inside primitive cell is shown in Fig. 1**b**. The refractive indices of the media surrounding the structure were denoted as $n_{04}$ for the medium adjacent to the loss layer and as $n_{01}$ for the medium next to the gain layer.

The complex amplitudes of the electromagnetic waves traveling in opposite directions in the gain and loss layers of the $n$-th primitive cell are denoted respectively: $(a_n, b_n)$, $(c_n, d_n)$, $(e_n, f_n)$ and $(g_n, h_n)$ [12], see Fig. 1**a**. The gain and loss layers are described by the small-signal gain coefficients $g_1$ and $g_2$, and small-signal loss coefficients $\alpha_3$ and $\alpha_4$, respectively.

The imaginary parts of the refractive indices of the gain layers are related to the small-signal gain coefficients, while the imaginary parts of the refractive indices of the loss layers are related to the small-signal loss coefficients. In nonlinear parity-time symmetric four-layer Bragg grating, it is necessary to take into account the gain and loss saturation effect. The imaginary parts will evolve in each layer depending on the distribution of the longitudinal field and the saturation intensity. To determine them, it is assumed that each layer of a primitive cell can be divided into very thin sublayers (see Fig. 1**c**). In each sublayer, the imaginary parts of the refractive indices $n_{1I}^{(i)}$, $n_{2I}^{(i)}$, $n_{3I}^{(i)}$, and $n_{4I}^{(i)}$ have the following forms:

$$n_{1I}^{(i)} = \frac{g_1/k_0}{1 + \frac{1}{I_{gs}}\left(\left|a_n^{(i)}\right|^2 + \left|b_n^{(i)}\right|^2\right)}, \quad n_{2I}^{(i)} = \frac{g_2/k_0}{1 + \frac{1}{I_{gs}}\left(\left|c_n^{(i)}\right|^2 + \left|d_n^{(i)}\right|^2\right)} \tag{2a}$$

$$n_{3I}^{(i)} = \frac{\alpha_3/k_0}{1 + \frac{1}{I_{\alpha s}}\left(\left|e_n^{(i)}\right|^2 + \left|f_n^{(i)}\right|^2\right)}, \quad n_{4I}^{(i)} = \frac{\alpha_4/k_0}{1 + \frac{1}{I_{\alpha s}}\left(\left|g_n^{(i)}\right|^2 + \left|h_n^{(i)}\right|^2\right)} \tag{2b}$$

where $k_0$ is the wavelength number in vacuum corresponding to the studied wavelength, $(a_n^{(i)}, b_n^{(i)})$, $(c_n^{(i)}, d_n^{(i)})$, $(e_n^{(i)}, f_n^{(i)})$ and $(g_n^{(i)}, h_n^{(i)})$ are electromagnetic field complex amplitudes for the $i$-th sublayer of the $n$-th PT primitive cell. These amplitudes are normalized in such a way that the formulas $(\left|a_n^{(i)}\right|^2 + \left|b_n^{(i)}\right|^2)$, $(\left|c_n^{(i)}\right|^2 + \left|d_n^{(i)}\right|^2)$, $(\left|e_n^{(i)}\right|^2 + \left|f_n^{(i)}\right|^2)$ and $(\left|g_n^{(i)}\right|^2 + \left|h_n^{(i)}\right|^2)$ describe the total wave intensity in each sublayer, respectively. $I_{gs}$ and $I_{\alpha s}$ are the saturation intensities in the gain and loss layers, respectively. Moreover, $Q$ is the number of sublayers in each primitive cell layer. Its

value determines the accuracy of the method and should be large enough to justify the assumption that the imaginary parts $n_{1I}^{(i)}$, $n_{2I}^{(i)}$, $n_{3I}^{(i)}$, and $n_{4I}^{(i)}$ are almost constant within corresponding sublayers. However, in the case of a linear structure where the gain and loss saturation effects are neglected, equations of the refractive indices' imaginary parts simplify to the numerator only (denominator equals unity).

Assuming the normal incidence of the wave on the edge of the PT structure, the transfer matrix describing the examined structure will be given by the matrix $M^{(\alpha,\,g)}$, where the superscript (α) denotes the incidence on the loss layer with the refractive index $n_4$, and the superscript (g) on the gain layer with the coefficient $n_1$. The transfer matrix $M^{(\alpha,\,g)}$ for $N > 1$, can be written as:

$$M^{(\alpha)} = J_{01}\left(\prod_{1}^{N-1} P_1 J_{12} P_2 J_{23} P_3 J_{34} P_4 J_{41}\right) P_1 J_{12} P_2 J_{23} P_3 J_{34} P_4 J_{40} \tag{3a}$$

$$M^{(g)} = J_{04}\left(\prod_{1}^{N-1} P_4 J_{43} P_3 J_{32} P_2 J_{21} P_1 J_{14}\right) P_4 J_{43} P_3 J_{32} P_2 J_{21} P_1 J_{10} \tag{3b}$$

where $P$ are the matrices describing the propagation of an electromagnetic wave inside one layer of the primitive cell and $J$ are the transfer matrices describing the behavior of the electromagnetic wave at the boundary between two layers.

The matrices $P$ will be different in each $i$-th sublayer of all layers of the PT primitive cell due to the modification of the longitudinal field resulting from changes in the imaginary parts of the refractive indices. For the $i$-th sublayer they have the following forms:

$$P_k^{(i)} = \begin{bmatrix} \exp\left[-jk_0(n_{kR} \mp jn_{kI}^{(i)})a/Q\right] & 0 \\ 0 & \exp\left[jk_0(n_{kR} \mp jn_{kI}^{(i)})a/Q\right] \end{bmatrix} \tag{4}$$

where $k$ is the number of the PT structure layers, the minus sign applies to the gain layers ($k = 1, 2$) and the plus sign to the loss ones ($k = 3, 4$). The matrices $P_k^{(i)}$ in each $i$-th sublayer are related to complex field amplitudes in adjacent sublayers:

$$\begin{bmatrix} a_n^{(i-1)} \\ b_n^{(i-1)} \end{bmatrix} = P_1^{(i)} \begin{bmatrix} a_n^{(i)} \\ b_n^{(i)} \end{bmatrix}, \quad \begin{bmatrix} c_n^{(i-1)} \\ d_n^{(i-1)} \end{bmatrix} = P_2^{(i)} \begin{bmatrix} c_n^{(i)} \\ d_n^{(i)} \end{bmatrix} \tag{5a}$$

$$\begin{bmatrix} e_n^{(i-1)} \\ f_n^{(i-1)} \end{bmatrix} = P_3^{(i)} \begin{bmatrix} e_n^{(i)} \\ f_n^{(i)} \end{bmatrix}, \quad \begin{bmatrix} g_n^{(i-1)} \\ h_n^{(i-1)} \end{bmatrix} = P_4^{(i)} \begin{bmatrix} g_n^{(i)} \\ h_n^{(i)} \end{bmatrix} \tag{5b}$$

The matrices $P_k$ are the products of all sublayers' elementary matrices:

$$\begin{bmatrix} a_n^{(0)} \\ b_n^{(0)} \end{bmatrix} = \prod_{i=1}^{Q} P_1^{(i)} \begin{bmatrix} a_n^{(Q)} \\ b_n^{(Q)} \end{bmatrix} = P_1 \begin{bmatrix} a_n^{(Q)} \\ b_n^{(Q)} \end{bmatrix} \tag{6a}$$

$$\begin{bmatrix} c_n^{(0)} \\ d_n^{(0)} \end{bmatrix} = \prod_{i=1}^{Q} P_2^{(i)} \begin{bmatrix} c_n^{(Q)} \\ d_n^{(Q)} \end{bmatrix} = P_2 \begin{bmatrix} c_n^{(Q)} \\ d_n^{(Q)} \end{bmatrix} \tag{6b}$$

$$\begin{bmatrix} e_n^{(0)} \\ f_n^{(0)} \end{bmatrix} = \prod_{i=1}^{Q} P_3^{(i)} \begin{bmatrix} e_n^{(Q)} \\ f_n^{(Q)} \end{bmatrix} = P_3 \begin{bmatrix} e_n^{(Q)} \\ f_n^{(Q)} \end{bmatrix} \tag{6c}$$

$$\begin{bmatrix} g_n^{(0)} \\ h_n^{(0)} \end{bmatrix} = \prod_{i=1}^{Q} P_4^{(i)} \begin{bmatrix} g_n^{(Q)} \\ h_n^{(Q)} \end{bmatrix} = P_4 \begin{bmatrix} g_n^{(Q)} \\ h_n^{(Q)} \end{bmatrix} \tag{6d}$$

The matrices $J$ link the fields at the boundaries of the layers:

$$\begin{bmatrix} a_0 \\ b_0 \end{bmatrix} = J_{04} \begin{bmatrix} g_1^{(0)} \\ h_1^{(0)} \end{bmatrix}, \quad \begin{bmatrix} a_{n-1}^{(Q)} \\ b_{n-1}^{(Q)} \end{bmatrix} = J_{14} \begin{bmatrix} g_n^{(0)} \\ h_n^{(0)} \end{bmatrix}, \quad \begin{bmatrix} g_n^{(Q)} \\ h_n^{(Q)} \end{bmatrix} = J_{43} \begin{bmatrix} e_n^{(0)} \\ f_n^{(0)} \end{bmatrix} \tag{7a}$$

$$\begin{bmatrix} e_n^{(Q)} \\ f_n^{(Q)} \end{bmatrix} = J_{32} \begin{bmatrix} c_n^{(0)} \\ d_n^{(0)} \end{bmatrix}, \quad \begin{bmatrix} c_n^{(Q)} \\ d_n^{(Q)} \end{bmatrix} = J_{21} \begin{bmatrix} a_n^{(0)} \\ b_n^{(0)} \end{bmatrix}, \quad \begin{bmatrix} a_N^{(Q)} \\ b_N^{(Q)} \end{bmatrix} = J_{10} \begin{bmatrix} g_{N+1} \\ 0 \end{bmatrix} \tag{7b}$$

$$\begin{bmatrix} g_1^{(0)} \\ h_1^{(0)} \end{bmatrix} = J_{40} \begin{bmatrix} 0 \\ b_0 \end{bmatrix}, \quad \begin{bmatrix} e_n^{(0)} \\ f_n^{(0)} \end{bmatrix} = J_{34} \begin{bmatrix} g_n^{(Q)} \\ h_n^{(Q)} \end{bmatrix}, \quad \begin{bmatrix} c_n^{(0)} \\ d_n^{(0)} \end{bmatrix} = J_{23} \begin{bmatrix} e_n^{(Q)} \\ f_n^{(Q)} \end{bmatrix} \tag{7c}$$

$$\begin{bmatrix} a_n^{(0)} \\ b_n^{(0)} \end{bmatrix} = J_{12} \begin{bmatrix} c_n^{(Q)} \\ d_n^{(Q)} \end{bmatrix}, \quad \begin{bmatrix} g_n^{(0)} \\ h_n^{(0)} \end{bmatrix} = J_{41} \begin{bmatrix} a_{n-1}^{(Q)} \\ b_{n-1}^{(Q)} \end{bmatrix}, \quad \begin{bmatrix} g_{N+1} \\ h_{N+1} \end{bmatrix} = J_{01} \begin{bmatrix} a_N^{(Q)} \\ b_N^{(Q)} \end{bmatrix} \tag{7d}$$

The calculation procedure of the output wave intensity $I_{\text{out}}^{(\alpha,\,g)}$ of the parity-time symmetric four-layer Bragg structure as a function of the incident plane wave intensity $I_{\text{in}}$, should be as follows. This procedure will be presented for the PT structure excited by the wave only on the loss layer with the refractive index $n_4$:

1. Select the parameters of the examined structure: the number of primitive cells $N$, the ratio of the PT structure period to operating wavelength $\Lambda/\lambda$ and the value of the

modulated refractive index real part $\Delta n_{\mathrm{R}}$. Set the values of saturation intensity $I_{\mathrm{gs}}$ and $I_{\alpha\mathrm{s}}$ for the investigated material in the gain and loss layers, respectively.

2. Divide each layer of PT primitive cell into as many sublayers as needed to assume that the gain or loss, for each one of the sublayers, is constant. $Q$ is the number of the sublayers. The width of a single sublayer is $l^{(i)}$ and is the same for all sublayers in the structure, $l^{(i)} = a/Q = b/Q = c/Q = d/Q$, where each sublayer is numbered by $i$.

3. Assuming that the wave is incident on the structure only on the loss layer ($h_{N+1} = 0$), set up the value of the output field complex amplitude as $I_{\mathrm{out}}^{(\mathrm{g})} = \left|g_{N+1}\right|^2$.

4. Using Eq. (7), calculate the amplitudes $a_N$ and $b_N$ in the $N$-th gain layer next to the structure boundary with the medium which refractive index is $n_{01}$. On the right sublayer boundary for $i = Q$, the wave amplitudes are $a_n^{(Q)} = a_N$, $b_n^{(Q)} = b_N$, (Fig. 1).

5. Using the previously calculated amplitudes on the right boundary $a_n^{(Q)}$ and $b_n^{(Q)}$, calculate the amplitudes $a_n^{(Q-1)}$ and $b_n^{(Q-1)}$ in the adjacent sublayer with Eq. (5). In the same way, using Eq. (5), determine the amplitudes $a_n^{(i-1)}$ and $b_n^{(i-1)}$ in the next sublayer, until the amplitudes $a_n^{(0)}$ and $b_n^{(0)}$ on the left border of the layer with the refractive index $n_1$ are obtained. This way, the distribution of wave amplitudes in the gain layer with the index $n_1$ will be iteratively calculated.

6. Using amplitudes $a_n^{(0)}$ and $b_n^{(0)}$ in Eq. (7), calculate the amplitudes $c_n^{(Q)}$ and $d_n^{(Q)}$ in the gain layer with the refractive index $n_2$ next to the border of the gain layer having the refractive index $n_1$.

7. Next, similarly to point 5 of this procedure, using Eq. (5), calculate the amplitudes $c_n^{(Q-1)}$ and $d_n^{(Q-1)}$ in the adjacent sublayer of the layer with the refractive index $n_2$. Successively calculate the amplitudes $c_n^{(i-1)}$ and $d_n^{(i-1)}$ in the following sublayers until the amplitudes $c_n^{(0)}$ and $d_n^{(0)}$ are obtained on the left layer boundary.

8. Using amplitudes $c_n^{(0)}$ and $d_n^{(0)}$ in Eq. (7), calculate the amplitudes $e_n^{(Q)}$ and $f_n^{(Q)}$ in the loss layer with the index $n_3$ next to the border of the gain layer with the index $n_2$. Similarly to point 5 and using Eq. (5), calculate the amplitudes $e_n^{(Q-1)}$ and $f_n^{(Q-1)}$, next $e_n^{(i-1)}$ and $f_n^{(i-1)}$ for subsequent sublayers to obtain the amplitudes $e_n^{(0)}$ and $f_n^{(0)}$.

9. Next, using amplitudes $e_n^{(0)}$ and $f_n^{(0)}$ in Eq. (7), calculate the amplitudes $g_n^{(Q)}$ and $h_n^{(Q)}$ in the loss layer with the index $n_4$ next to the border with the loss layer with the index $n_3$. Similarly to point 5 of this procedure and using Eq. (5), calculate the amplitudes $g_n^{(Q-1)}$ and $h_n^{(Q-1)}$, next $g_n^{(i-1)}$ and $h_n^{(i-1)}$ for successive sublayers, until the amplitudes $g_n^{(0)}$ and $h_n^{(0)}$ are obtained.

10. If the layer with the refractive index $n_4$ borders the layer with the index $n_1$, using amplitudes $g_n^{(0)}$ and $h_n^{(0)}$ in Eq. (7), determine the amplitudes $a_{n-1}^{(Q)}$ and $b_{n-1}^{(Q)}$.

11. Repeat the calculations from points 5 to 10, until the field amplitudes in all layers of the whole PT structure are determined.

12. Using amplitudes $g_1^{(0)}$ and $h_1^{(0)}$ in Eq. (7), calculate the amplitudes $a_0$ and $b_0$ in the medium with the refractive index $n_{04}$ next to the PT structure's left boundary. The latter are amplitudes of the incident and reflected waves, which allow to determine those waves' intensities, respectively: $I_{\mathrm{in}} = |a_0|^2$ and $I_{\mathrm{r}} = |b_0|^2$.

Starting at step 3 of the procedure above, the calculation process can be repeated for the next $I_{\text{out}}^{(\text{g})} = \left|g_{N+1}\right|^2$. In the case when the PT structure is excited only from the gain side with the refractive index $n_1$, the procedure of determining the intensity of the output wave $I_{\text{out}}^{(\alpha)}$ is analogous to the presented one.

## 3. Numerical results

Numerical analysis of the parity-time symmetric four-layer Bragg grating structure was carried out with the assumption that the constant component of the refractive index's real part is equal to $n_0 = 3.165$. It was also carried out for four configurations related to the materials surrounding the analyzed system: the first for $n_{01} = n_{04} = 1$, the second $n_{01} = n_{04} = 3.165$, the third $n_{01} = 1$, $n_{04} = 3.165$ and the fourth $n_{01} = 3.165$, $n_{04} = 1$. The absolute value of the numerator of the refractive indices' imaginary parts in all layers is 0.1, $|g_1/k_0| = |g_2/k_0| = |\alpha_3/k_0| = |\alpha_4/k_0| = 0.1$ (a more detailed analysis of the linear PT structure for different values of $n_{\text{I}}$ is presented in [17]). According to Eq. (1), the modulation of the refractive index's real part is obtained by changing the constant component $n_0$ by the parameter $\Delta n_{\text{R}}$. The value $\Delta n_{\text{R}}$ was selected based on [18] and it can be up to 0.055 for InP.

The nonlinear analysis of the four-layer PT structure is performed for geometrical parameters (the number $N$ of primitive cells and the ratio of the grating period to the operating wavelength $\Lambda/\lambda$), which provide the highest values of the reflectivity coefficient. To determine these parameters, it is necessary to investigate the reflection $\left|r_N^{(\alpha,\,\text{g})}\right|^2$ and transmission coefficients $\left|t_N^{(\alpha,\,\text{g})}\right|^2$ of the linear PT structure for which the gain and loss saturation effects are neglected. These coefficients are calculated using the transfer matrix method presented in [12]. Additionally, it has been investigated whether the four-layer structures meet the PT symmetry conditions [12].

The Table presents the highest maxima of the reflection coefficients from the loss layer $\left|r_N^{(\alpha)}\right|^2$ and the gain layer $\left|r_N^{(\text{g})}\right|^2$, and transmission coefficients $\left|t_N^{(\alpha,\,\text{g})}\right|^2$ for four configurations with adequate values of the number $N$, the ratio $\Lambda/\lambda$ and the length $L$ of the whole structure. It also includes information about meeting the PT symmetry conditions. In order to provide the miniaturization of the PT systems and facilitate their production, only the results for the smallest number of cells $N$ are shown.

In the configuration I, the values in the Table indicate that with the increase of the parameter $\Delta n_{\text{R}}$, the magnitude of the largest maxima of reflection and transmission coefficients increases. The lack of modulation of the refractive index's real part ($\Delta n_{\text{R}} = 0$) corresponds to a two-layer primitive cell of the PT structure. The introduction of the modulation $\Delta n_{\text{R}} = 0.0001$ results in a change in the configuration of the primitive cell (from two-layer to four-layer) and an increase of reflection and transmission coefficients, while maintaining the number $N$ and the ratio $\Lambda/\lambda$. A further increase of $\Delta n_{\text{R}}$ causes an increase of reflection and transmission coefficients, and a decrease in $\Lambda/\lambda$ with a simultaneous increase in $N$ (which results in a decrease of the investigated structure length $L$).

T a b l e. Linear PT structure parameters for all configurations.

| Conf.* | $\Delta n_R$ | $\Lambda/\lambda$ | $N$ | $L$ [μm] | $\left\|r_N^{(\alpha)}\right\|^2$ | $\left\|r_N^{(g)}\right\|^2$ | $\left\|t_N^{(\alpha,\,g)}\right\|^2$ | PT sym. cond.** |
|---|---|---|---|---|---|---|---|---|
| I | 0.0 | 1.4204740 | 21 | 46.24 | 8079.58 | 21383.10 | 13145.10 | broken |
| I | 0.0001 | 1.4204713 | 21 | 46.24 | 8887.79 | 23574.40 | 14475.90 | broken |
| I | 0.001 | 1.4204474 | 21 | 46.24 | 28258.00 | 76462.80 | 46484.10 | broken |
| I | 0.01 | 1.1051379 | 23 | 39.40 | 150843.00 | 267395.00 | 200836.00 | broken |
| II | 0.0 | 0.7898890 | 24 | 29.38 | 10061.80 | 27163.30 | 16533.10 | broken |
| II | 0.0001 | 0.7898890 | 24 | 29.38 | 10040.20 | 27211.20 | 16529.90 | broken |
| II | 0.001 | 0.7898888 | 24 | 29.38 | 9677.95 | 27168.50 | 16216.30 | broken |
| II | 0.01 | 0.1579765 | 25 | 6.12 | 120810.00 | 220105.00 | 163064.00 | broken |
| III | 0.0 | 0.4719890 | 21 | 15.36 | 69583.41 | 35842.79 | 50089.63 | none |
| III | 0.0001 | 0.4719902 | 21 | 15.36 | 59249.20 | 30414.70 | 42587.90 | none |
| III | 0.001 | 0.7876852 | 20 | 24.42 | 459771.00 | 324001.00 | 386389.00 | none |
| III | 0.01 | 1.4187129 | 17 | 37.38 | 45345.00 | 64623.40 | 53958.20 | none |
| IV | 0.0 | 1.1070812 | 22 | 37.75 | 13849300.00 | 134823000.00 | 43214900.00 | none |
| IV | 0.0001 | 1.1070821 | 22 | 37.75 | 1143690000.0 | 11096800000.0 | 3562280000.0 | none |
| IV | 0.001 | 1.1070898 | 22 | 37.75 | 147502.00 | 1387580.00 | 452017.00 | none |
| IV | 0.01 | 1.1071736 | 22 | 37.76 | 2917.74 | 20330.80 | 7651.11 | none |

*Conf. – configuration; **PT sym. cond. – PT symmetry conditions

The values in the Table for the configuration II show that the increase of the parameter $\Delta n_R$, causes strong increase of the reflection and transmission coefficients for $\Delta n_R = 0.01$ only, while increasing the number $N$, decreasing the ratio $\Lambda/\lambda$, and simultaneously decreasing the structure length $L$. In the configurations III and IV, a significant increase of the reflection and transmission coefficients is observed for $\Delta n_R = 0.001$ and $\Delta n_R = 0.0001$, respectively. Moreover, the highest maxima of the reflection and transmission coefficients are obtained for the fourth configuration with a slight change of the refractive index's real part's modulation parameter $\Delta n_R$. Additionally, in this configuration, the increase of the parameter $\Delta n_R$ does not change any of the following parameters: the number $N$, the ratio $\Lambda/\lambda$ and the length $L$. Comparing the results obtained for presented PT structure configurations shows that in configurations I, II, and IV, higher reflection coefficients were obtained for the case when the electromagnetic wave is incident on the gain layer. This effect was considered theoretically [2] and confirmed experimentally for PT metamaterials [19].

The Table indicates that for configurations I and II, the investigated structures meet the PT symmetry breaking conditions. In these configurations, the PT structures are surrounded on both sides by a material of the same refractive index, $n_{01} = n_{04} = 1$ for the first configuration and $n_{01} = n_{04} = 3.165$ for the second one. However, for configurations III and IV, none of the symmetry and symmetry breaking conditions are met. In this case, the structures are surrounded by two different materials: $n_{01} \neq n_{04}$. More-

over, for all configurations, rows in the Table corresponding to the highest reflection and transmission are marked in gray.

The nonlinear analysis includes gain and loss saturation effects in the PT four-layer structure according to Eq. (2). The characteristics of the output wave intensity as a function of the incident wave intensity were obtained using the procedure presented in the previous chapter. The intensity $I_{\mathrm{out}}^{(\mathrm{g})}$ leaves the PT structure through the gain layer, when the input wave is incident on the loss side of the PT structure. The intensity $I_{\mathrm{out}}^{(\alpha)}$ escapes from the loss layer, when the input wave is incident on the gain side. Figures 2–5 show

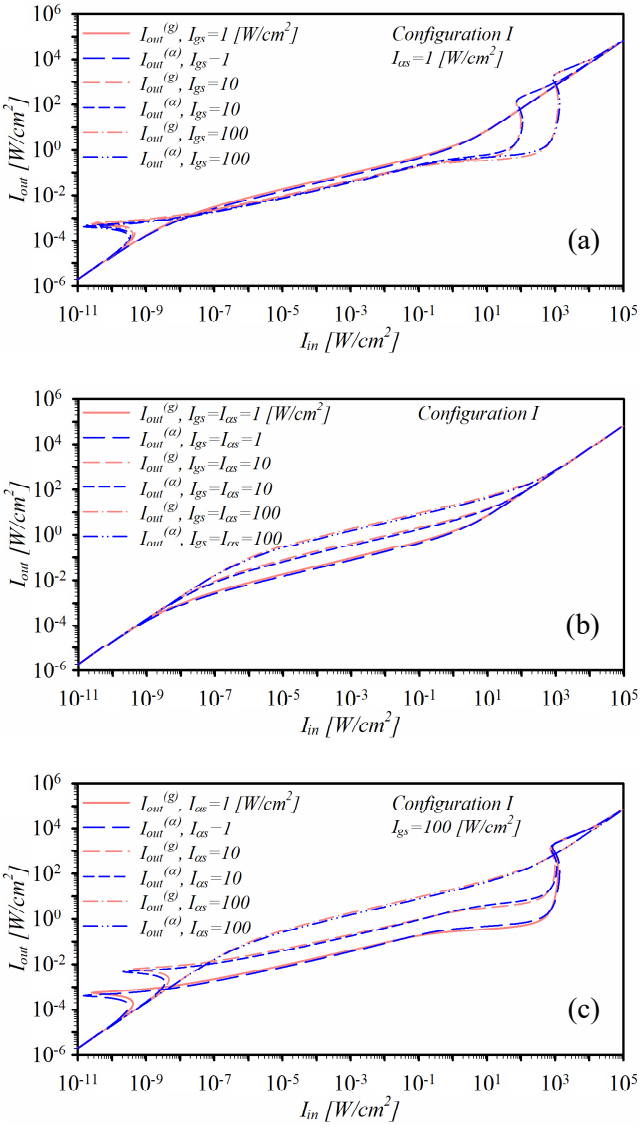


Fig. 2. Output wave intensity as a function of the incident wave intensity for configuration I.

the output intensity $I_{out}^{(g)}$ and $I_{out}^{(\alpha)}$ for all configurations. Investigations were carried out for different sets of saturation values of the gain $I_{gs}$ and loss $I_{\alpha s}$: (a) $I_{\alpha s}$ = 1 W/cm$^2$ and $I_{gs}$ = 1, 10, 100 W/cm$^2$; (b) $I_{gs} = I_{\alpha s}$ = 1, 10, 100 W/cm$^2$; (c) $I_{gs}$ = 100 W/cm$^2$ and $I_{\alpha s}$ = 1, 10, 100 W/cm$^2$. In general, as expected, the output wave intensity increases with increasing of the incident wave intensity similar to typical active structures. Moreover, the change of the gain and loss saturation intensity does not affect the output wave intensity for very small ($I_{in} < 10^{-9}$ W/cm$^2$) and very large ($I_{in} > 10^3$ W/cm$^2$) values of the incident wave intensities, causing the characteristics to overlap in the indicated

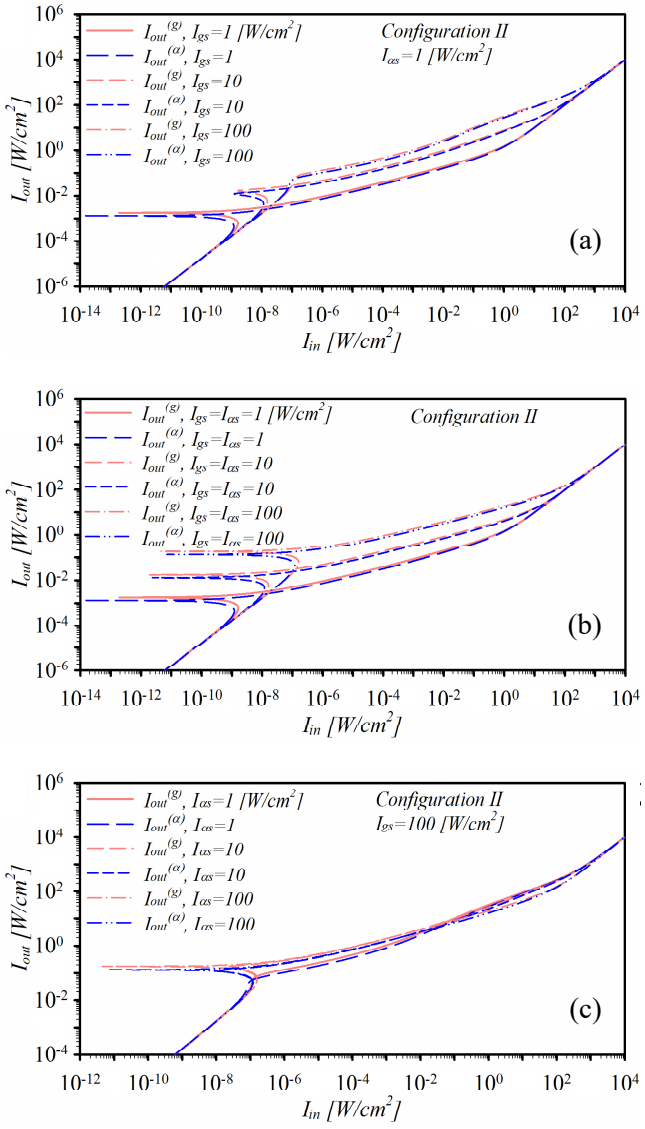


Fig. 3. Output wave intensity as a function of the incident wave intensity for configuration II.

ranges. In the case of low incident wave intensities, it is related to negligibly low saturation of the PT structure layers. In the case of high values of incident wave intensity, it results from strong saturation of the layers of the examined structure, which causes vanishing of the gain and loss effect.

The curves presented in Fig. 2 (first configuration) show that the intensity of the waves leaving the PT structure through the gain and loss layers are the same for the same sets of saturation intensity values. In the case of $I_{\alpha s} = 1$ W/cm$^2$, Fig. 2**a** for a middle range of the input wave intensity $10^{-9}$ W/cm$^2$ < $I_{in}$ < $10^3$ W/cm$^2$, it can be observed

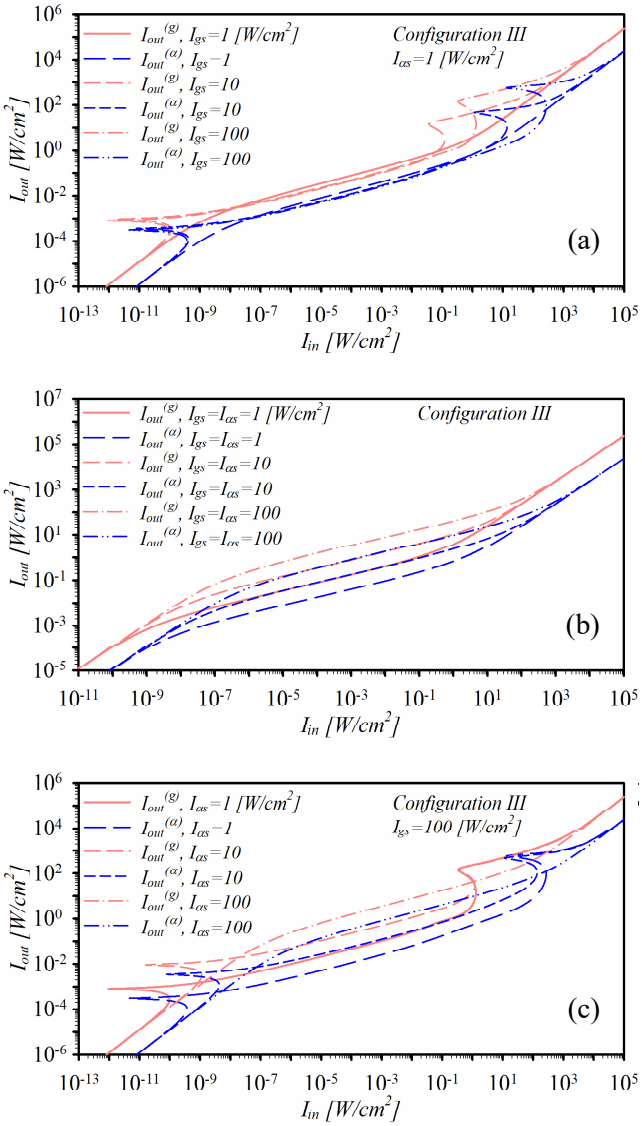


Fig. 4. Output wave intensity as a function of the incident wave intensity for configuration III.

that the output wave intensity $I_{out}^{(\alpha,\,g)}$ decreases with increasing saturation $I_{gs}$. However, for higher values of $I_{\alpha s}$, Figs. 2**b** and 2**c**, the output wave intensity increases with increasing saturation $I_{gs}$, because the gain layer saturates more slowly. A bistability effect occurs when the saturation intensity of the gain layer is greater than the saturation of loss layer ($I_{gs} > I_{\alpha s}$), which is caused by the loss layer saturating faster. Moreover, the bistability appears on one curve in two areas, for very low and very high values of the incident wave intensity.

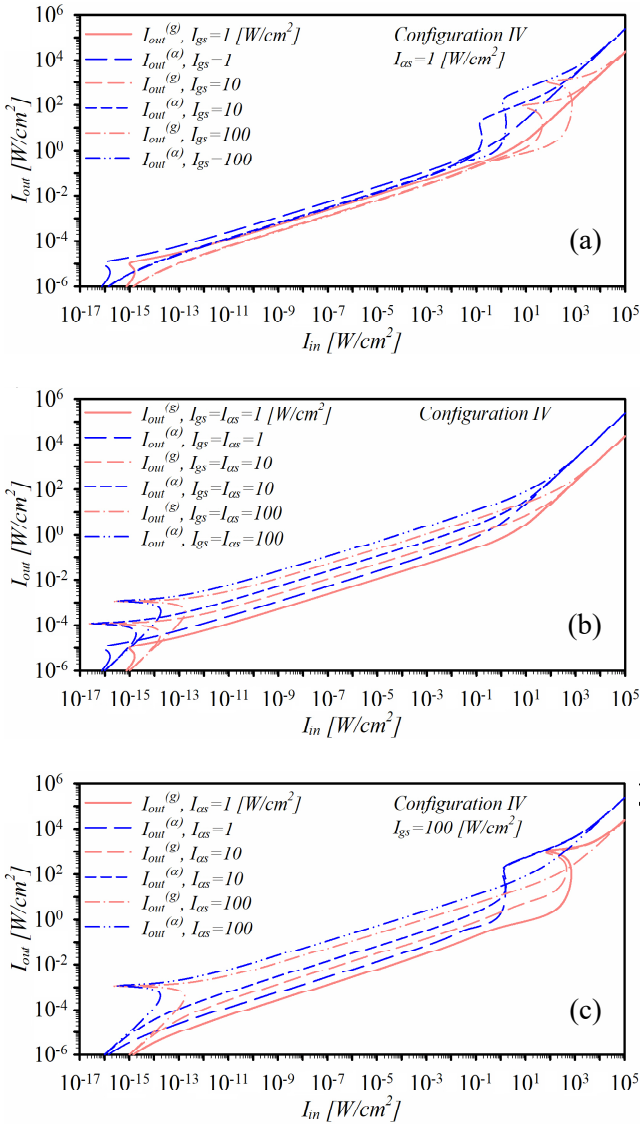


Fig. 5. Output wave intensity as a function of the incident wave intensity for configuration IV.

Figure 3 shows the characteristics for configuration II, when the PT structure is surrounded by a semiconductor. In Figs. 3**a** and 3**b**, an increase of the saturation $I_{gs}$ causes an increase of the output intensity $I_{out}^{(\alpha, g)}$. However, in Fig. 3**c**, for constant value of the saturation $I_{gs}$, an increase of the saturation $I_{\alpha s}$ slightly modifies the output wave intensity characteristics. As shown for configuration I, bistability is observed only when $I_{gs} > I_{\alpha s}$. However, this effect is stronger, because the hysteresis loop is wider.

Figure 4 contains the characteristics of the output wave intensity $I_{out}^{(\alpha, g)}$ as a function of the incident wave intensity $I_{in}$ for the case of configuration III, where the loss layer is adjacent to the medium with a high refractive index and the gain layer is adjacent to the air. For all sets of the saturation intensities $I_{\alpha s}$ and $I_{gs}$, the behavior of the output intensity is similar to that presented in Fig. 2. However, a comparison of the output intensity values of the waves leaving the structure through the gain and loss layers, shows that the wave intensity $I_{out}^{(g)}$ is greater than the intensity $I_{out}^{(\alpha)}$ for the same input intensity $I_{in}$. The bistability effect, similarly to Fig. 2, occurs when the saturation intensity of the gain layer is greater than that of the loss layer ($I_{gs} > I_{\alpha s}$).

The curves presented in Fig. 5 were plotted for the fourth configuration, where the gain layer is adjacent to the medium with a high refractive index and the loss layer is adjacent to the air. The obtained intensity of the waves leaving the structure through the loss layer into the air is greater than of those leaving through the gain layer into the semiconductor. Moreover, for a constant value of the saturation intensity $I_{\alpha s}$, the change of the output wave intensity as a function of the saturation intensity $I_{gs}$ is the same as for the first configuration. The bistability effect occurs on all presented curves, but there is only one hysteresis loop per curve.

## 4. Conclusions

This work presents the output wave intensity of the PT four-layer Bragg structure as a function of the wave intensity incidents on the structure with the modulated refractive index. The real part of the refractive index of the gain and loss layers, which create the primitive cell of the investigated system, was modulated. Studying the PT structure's transmission properties allowed to indicate geometrical parameters: the ratio of the PT structure period to the operating wavelength $\Lambda/\lambda$ and the number of primitive cells $N$. These parameters were used in the nonlinear analysis of the PT structure operating as a discrete device or a component of an integrated optoelectronics system. This analysis calculated the output wave intensity of the PT structure for four configurations by using the modified transfer matrix method and taking into account gain and loss saturation effects.

The obtained characteristics illustrate the effect of the gain and loss saturation of the output wave $I_{out}^{(\alpha, g)}$ at a given incident wave intensity $I_{in}$. The results demonstrate a strong influence of the gain and loss saturation effect on the output wave intensity in all analyzed configurations. In particular, these effects vary the output wave intensities only for the input wave intensities in the range $10^{-9}$ W/cm$^2$ $< I_{in} <$ $10^3$ W/cm$^2$. For small values of the loss saturation intensity $I_{\alpha s}$, the output wave intensity decreases

with increasing of the gain saturation intensity. The opposite situation takes place for higher values of $I_{\alpha s}$, where the output wave intensity increases with increasing of the gain saturation intensity $I_{gs}$.

The media surrounding the structure affect the value of the output wave intensity showing a strong influence on the properties of light propagation nonreciprocity. In the first and second configuration (where the PT structure is surrounded by air or a semiconductor, respectively), for the same sets of saturation intensity values, the output intensities are independent of the layer type (gain or loss) through which the wave leaves the structure. The contrary behavior is observed in the third and fourth configurations, where the PT structure is surrounded by two different media. For the same sets of saturation intensity values, the output wave intensities are greater when the wave leaves the structure through the boundaries of media with a greater variation of refraction indices.

The presented characteristics show the bistability effect in the PT structure. In all configurations, the bistability is observed when the gain saturation intensity $I_{gs}$ is greater than the loss saturation intensity $I_{\alpha s}$. Moreover, it occurs for two ranges of the incident wave intensities: $I_{in} < 10^{-8}$ W/cm$^2$ and $I_{in} > 10^{0}$ W/cm$^2$. However, for the third configuration, it appears only for lower range of $I_{in}$. Additionally, when the gain saturation intensity is equal to the loss saturation intensity, the bistability effect is present only in the second and fourth configuration. In these cases, the gain layer of the PT structure is adjoined to the semiconductor medium and variation of refraction indices on the media boundary is very small.

**Acknowledgements**
The authors wish to thank Miss Urszula Wyszyńska for checking linguistic correctness of the manuscript.

## References

[1] Bender C.M., Boettcher S., *Real spectra in non-Hermitian Hamiltonians having PT symmetry*, Physical Review Letters **80**(24), 1998, pp. 5243–5246, DOI: 10.1103/PhysRevLett.80.5243.

[2] Lin Z., Ramezani H., Eichelkraut T., Kottos T., Cao H., Christodoulides D.N., *Unidirectional invisibility induced by PT-symmetric periodic structures*, Physical Review Letters **106**(21), 2011, 213901, DOI: 10.1103/PhysRevLett.106.213901.

[3] Sun Y., Tan W., Li H., Li J., Chen H., *Experimental demonstration of a coherent perfect absorber with pt phase transition*, Physical Review Letters **112**(14), 2014, 143903, DOI: 10.1103/PhysRevLett.112.143903.

[4] Makris K.G., El-Ganainy R., Christodoulides D.N., Musslimani Z.H., *Beam dynamics in PT symmetric optical lattices*, Physical Review Letters **100**(10), 2008, 103904, DOI: 10.1103/PhysRevLett.100.103904.

[5] El-Ganainy R., Makris K.G., Christodoulides D.N., Musslimani Z.H., *Theory of coupled optical PT-symmetric structures*, Optics Letters **32**(17), 2007, pp. 2632–2634, DOI: 10.1364/OL.32.002632.

[6] Heinrich M., Miri M.-A., Khajavikhan M., Christodoulides D.N., *PT symmetry in optics and nonlinear optics*, Proceedings of 2015 European Conference on Lasers and Electro-Optics – European Quantum Electronics Conference, June 21–25, 2015, Munich, Germany, paper CD_3_4.

[7] Phang S., Vukovic A., Susanto H., Benson T.M., Sewell P., *Ultrafast optical switching using parity-time symmetric Bragg gratings*, Journal of the Optical Society of America B **30**(11), 2013, pp. 2984–2991, DOI: 10.1364/JOSAB.30.002984.

[8] KULISHOV M., LANIEL J.M., BÉLANGER N., AZAÑA J., PLANT D.V., *Nonreciprocal waveguide Bragg gratings*, Optics Express **13**(8), 2005, pp. 3068–3078, DOI: 10.1364/OPEX.13.003068.

[9] KULISHOV M., KRESS B., JONES H.F., *Novel optical characteristics of a Fabry-Perot resonator with embedded PT-symmetrical grating*, Optics Express **22**(19), 2014, pp. 23164–23181, DOI: 10.1364/OE.22.023164.

[10] GE L., EL-GANAINY R., *Nonlinear modal interactions in parity-time* (*PT*) *symmetric lasers*, Scientific Reports **6**, 2016, 24889, DOI: 10.1038/srep24889.

[11] MOSSAKOWSKA-WYSZYŃSKA A., NIEDŹWIEDZIUK P., WITOŃSKI P., SZCZEPAŃSKI P., *Analysis of light generation in laser with PT-symmetric mirror*, Proceedings Advanced Photonics 2018, July 2–5, 2018, Zurich, Switzerland, paper JTu5A.50, DOI: 10.1364/BGPPM.2018.JTu5A.50.

[12] WITOŃSKI P., MOSSAKOWSKA-WYSZYŃSKA A., SZCZEPAŃSKI P., *Effect of nonlinear loss and gain in multilayer PT-symmetric Bragg grating*, IEEE Journal of Quantum Electronics **53**(6), 2017, 8063405, DOI: 10.1109/JQE.2017.2761380.

[13] SMIT M., WILLIAMS K., VAN DER TOL J., *Past, present, and future of InP-based photonic integration*, APL Photonics **4**(5), 2019, 050901, DOI: 10.1063/1.5087862.

[14] SOARES F.M., BAIER M., GAERTNER T., GROTE N., MOEHRLE M., BECKERWERTH T., RUNGE P., SCHELL M., *InP-based foundry PICs for optical interconnects*, Applied Sciences **9**(8), 2019, 1588, DOI: 10.3390/app9081588.

[15] *Indium Phosphide PICs, 100G Optical Components*, Coherent, PIC, DWDM, <https://www.neophotonics.com/technology/indium-phosphide-pics/> (accessed May 23, 2019).

[16] PHANG S., *Theory and numerical modelling of parity-time symmetric structures for photonics*, 2016, <http://eprints.nottingham.ac.uk/32596/> (accessed November 30, 2018).

[17] MOSSAKOWSKA-WYSZYŃSKA A., WITOŃSKI P., SZCZEPAŃSKI P., *Transmission properties analysis of 1D PT-symmetric photonic structures*, Proc. SPIE **10175**, Electron Technology Conference 2016, 101750T, DOI: 10.1117/12.2260706.

[18] CHUSSEAU L., MARTIN P., BRASSEUR C., ALIBERT C., *Carrier-induced change due to doping in refractive index of InP: Measurements at 1.3 and 1.5 μm*, Applied Physics Letters **69**(20), 1996, pp. 3054–3056, DOI: 10.1063/1.116837.

[19] FENG L., XU Y.-L., FEGADOLLI W.S., LU M.-H., OLIVEIRA J.E.B., ALMEIDA V.R., CHEN Y.-F., SCHERER A., *Experimental demonstration of a unidirectional reflectionless parity-time metamaterial at optical frequencies*, Nature Materials **12**(2), 2013, pp. 108–113, DOI: 10.1038/nmat3495.

*Received February 9, 2021*
*in revised form June 7, 2021*